Superconductivity in palladium-based Heusler compounds

Jürgen Winterlik, Gerhard H. Fecher, Anja Thomas, and Claudia Felser
Institut für Anorganische und Analytische Chemie, Johannes Gutenberg-Universität, 55099 Mainz, Germany
(Received 5 September 2008; published 4 February 2009)

This work reports on four more Heusler superconductors: Pd_2ZrAl, Pd_2HfAl, Pd_2ZrIn, and Pd_2HfIn. These compounds exhibit superconducting transition temperatures ranging from 2.4–3.8 K as determined by resistivity measurements. According to their behavior in an external magnetic field, all compounds are type II bulk superconductors. The occurrence of superconductivity was predicted for these compounds using electronic structure calculations. The electronic structures exhibit van Hove singularities (saddle points) at the L point. These lead to a maximum in the corresponding density of states and superconductivity according to the van Hove scenario. The superconducting properties of electron-doped and hole-doped substituted compounds $Pd_2B_{1-x}B'_xAl$, whereby B=Zr and Hf, and B'=Y, Nb, and Mo, were investigated to obtain information about the dependence of the transition temperature on the density of states at the Fermi energy following the van Hove scenario. The calculated electronic structure reveals that the substituted compounds do not follow a rigid-band model. In addition, the random distribution of the substituted atoms strongly increases impurity-type electron scattering. The substituent concentrations used in this work lead to strongly enhanced impurity-type scattering and eventually to suppression of the superconducting state.

DOI: 10.1103/PhysRevB.79.064508 PACS number(s): 71.20.Be, 74.70.Ad, 75.20.En, 85.25.Cp

I. INTRODUCTION

Heusler compounds with the $L2_1$ structure type and a stoichiometric composition A_2BC became popular with the archetype Cu_2MnAl,[1] a remarkable compound that shows ferromagnetic ordering despite the absence of any ferromagnetic element. At present, the Heusler family is widely associated with the research area of spintronic applications. Some Heusler compounds have been reported to show half-metallic ferromagnetism,[2,3] a feature of utmost concern with respect to the desired high degree of spin polarization, and thus for implementation in spintronic applications. Several Co-based Heusler compounds were employed as electrodes in magnetic tunnel junctions.[4,5] In contrast to the magnetic Heusler compounds, Heusler superconductors play a minor role with respect to application because of their low transition temperatures. Investigating what causes a certain Heusler compound to show magnetic order or superconductivity is, however, of general scientific interest.

Up to now, very few Heusler compounds have been reported to be superconductors; the first of these were published in Ishikawa's pioneering review.[6] Currently, Pd_2YSn is the Heusler compound with the highest critical temperature T_c of 4.9 K.[7] Despite the occurrence of ferromagnetic ordering in elemental nickel, Heusler compounds with nickel at the Wyckoff 8c position were found to exhibit superconductivity; the compound with the currently highest critical temperature of 3.4 K, Ni_2NbSn, was reported in 1983.[7] The coexistence of superconductivity and antiferromagnetic order was found in Heusler compounds Pd_2YbSn (Ref. 8) and Pd_2ErSn.[9]

For a better understanding of the magnetic properties of solid materials, we need to understand their electronic structures. We have performed electronic structure calculations using *ab initio* methods in order to find promising palladium-based Heusler compounds as candidates for superconductivity that match our design criterion, i.e., a saddle point at a certain high-symmetry point in the energy dispersion curve at the Fermi energy ϵ_F. Such a saddle point leads to a high density of states $n(\epsilon_F)$ at the Fermi energy. These are referred to as van Hove singularities.[10] Prospective candidates for superconductivity include certain Heusler compounds with 27 electrons that exhibit a saddle point at the L point close to ϵ_F in the corresponding energy dispersion curve according to the van Hove scenario.[11–13] It is known from the BCS theory for superconductivity that the transition temperature of a superconducting material increases exponentially with an increasing $n(\epsilon_F)$ given that Debye frequency and Cooper-pairing interaction are independent of $n(\epsilon_F)$.[14] The unusually high transition temperatures of the intermetallic $A15$ superconductors, which are highly important for application purposes (i.e., as superconducting magnets), were explained with the van Hove scenario. Based on the van Hove scenario, we have already reported Heusler superconductors with 27 electrons: Pd_2ZrAl, Pd_2HfAl, and Ni_2ZrGa.[12,13] Here we present a more detailed investigation of the palladium-based compounds and report two more 27-electron superconducting Heusler compounds: Pd_2ZrIn and Pd_2HfIn. Electron-doping and hole-doping experiments were performed with Pd_2ZrAl and Pd_2HfAl to investigate the dependence of T_c on the energy of the corresponding van Hove singularities. To do this, we prepared and characterized solid solutions of pure compounds of $Pd_2B_{1-x}B'_xAl$, whereby B=Zr and Hf, and B'=Y, Nb, and Mo.

II. CALCULATIONAL DETAILS

The electronic and vibrational properties of the pure compounds were calculated by means of WIEN2k (Refs. 15 and 16) in combination with PHONON.[17] The electronic properties of the substituted—electron-doped or hole-doped—compounds were calculated using the Korringa-Kohn-Rostocker method together with the coherent-potential approximation.[18,19]

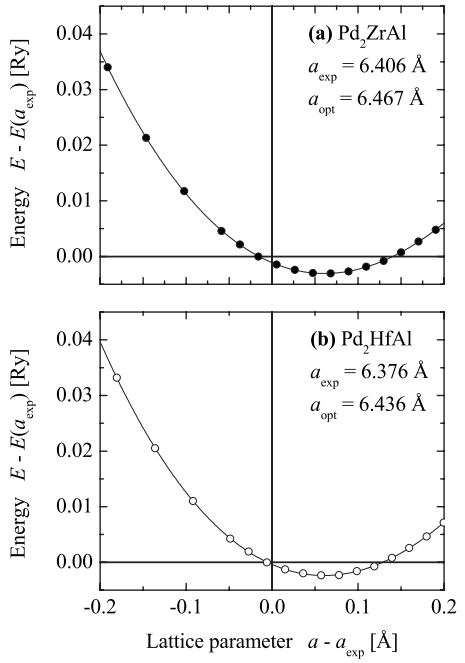

FIG. 1. Optimization of the lattice parameter. Shown is the optimization for Pd_2ZrAl in (a) and Pd_2HfAl in (b). The solid lines are the results of an equation of state fit.

The electronic structure of the pure A_2BC compounds was calculated using the full potential linearized augmented plane-wave (FLAPW) method as implemented in WIEN2k. The exchange-correlation functional was taken within the generalized gradient approximation (GGA).[20] A $25\times25\times25$ point mesh was used as basis for integration in the cubic systems resulting in 455 k points in the irreducible wedge of the Brillouin zone. The energy convergence criterion was set to 10^{-5} Ry while, at the same time, the criterion for charge convergence was set to $1\times10^{-3}e^-$. The muffin-tin radii were set to 2.5 a_{0B} (a_{0B}=0.529 177 2 Å) for the transition metals as well as the main group element. The primitive fcc cell, which contains four atoms, was enlarged to a cell with 16 distinguished atoms to calculate the Hellmann-Feynman forces for the phonon analysis. For these calculations, a force convergence criterion of 1×10^{-4} Ry a_{0B}^{-1} was used in addition to the energy and charge convergence criteria. All phonon calculations were performed for the optimized lattice parameter.

The electronic structure of the substituted $A_2B_{1-x}B'_xC$ compounds was calculated by means of the full relativistic Korringa-Kohn-Rostocker (SPRKKR) method.[18,19] The exchange-correlation functional was taken within the Vosko-Wilk-Nusair parametrization.[21,22] No noticeable differences in the electronic structure were observed when using the full potential version of the program together with GGA. The coherent-potential approximation (CPA) was used to account for the random distribution of the B and B' atoms in the $Pd_2B_{1-x}B'_xAl$ or $Pd_2B_{1-x}B'_xIn$ solid solutions.

The electronic structures reported below (see Sec. IV) were calculated for the experimental as well as the optimized lattice parameter of each compound. Figure 1 shows the results for the optimization of the lattice parameter for Pd_2ZrAl and Pd_2HfAl. The optimized lattice parameters from an equation of states fit[23] are slightly larger than experimental parameters by about 1%. This is common for calculations in the generalized gradient approximation. GGA slightly overestimates the lattice parameter compared to the pure local-density approximation, which tends to overbinding.[24–26] The accompanying bulk moduli for Pd_2ZrAl and Pd_2HfAl are 151 and 159 GPa, respectively. The results from the optimization of the lattice parameters are summarized in Table I.

TABLE I. Lattice parameters of palladium-based superconducting Heusler compounds. Compared are the experimental values a_{exp} (see Sec. IV) with the optimized values a_{opt}. B is the bulk modulus.

	a_{exp} (Å)	a_{opt} (Å)	B (GPa)
Pd_2ZrAl	6.406	6.467	151
Pd_2ZrIn	6.536	6.623	141
Pd_2HfAl	6.376	6.436	159
Pd_2HfIn	6.530	6.592	150

III. EXPERIMENTAL DETAILS

Polycrystalline ingots were prepared by repeated arc melting of stoichiometric mixtures of the elements in an argon atmosphere at a pressure of 1×10^{-4} mbar to avoid oxygen contamination. The samples were subsequently annealed for two weeks at 1073 K in evacuated quartz tubes. After the annealing process, the samples were quenched to 273 K in a mixture of ice and water to retain the desired $L2_1$ structure. Slow cooling of the samples after the annealing process leads to enhanced $B2$-type antisite disorder. This is mainly a disorder between the transition metal (B) on the 4a site with the main group element (C) on the 4b site that is often found in Heusler compounds.

The crystal structures of the compounds were investigated using powder x-ray diffraction (XRD). The XRD measurements were carried out using a Siemens D5000 diffractometer with monochromatized Cu K_α radiation. The purity of the compounds was confirmed using scanning electron microscopy with energy dispersive x-ray spectroscopy (EDX). The superconducting transitions were verified in resistivity measurements using a Physical Property Measurement System (PPMS, Quantum Design, Model 6000). The resistivity of samples with polished surfaces was measured using the four-point probe technique. The diamagnetic shielding and the Meissner effect of the compounds were investigated using temperature-dependent and field-dependent magnetization measurements with a superconducting quantum interference device (SQUID, Quantum Design, MPMS-XL-5). Small spherical sample pieces of approximately 20 to 120 mg were used to ensure precise measurements. The temperature-dependent magnetization measurements were carried out under zero-field-cooled (ZFC) and field-cooled (FC) conditions. For the ZFC measurements, the samples were first cooled down to 1.8 K without applying any magnetic field. Afterward, an external magnetic field of 2.5 mT

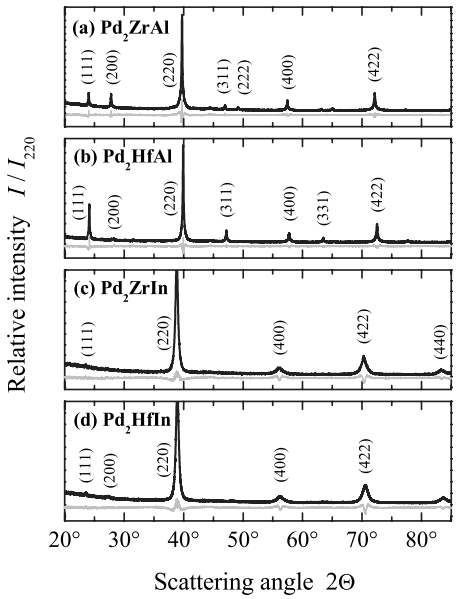

FIG. 2. X-ray diffraction patterns of the pure Heusler superconductors. Panels (a)–(d) display the patterns for Pd_2ZrAl, Pd_2HfAl, Pd_2ZrIn, and Pd_2HfIn.

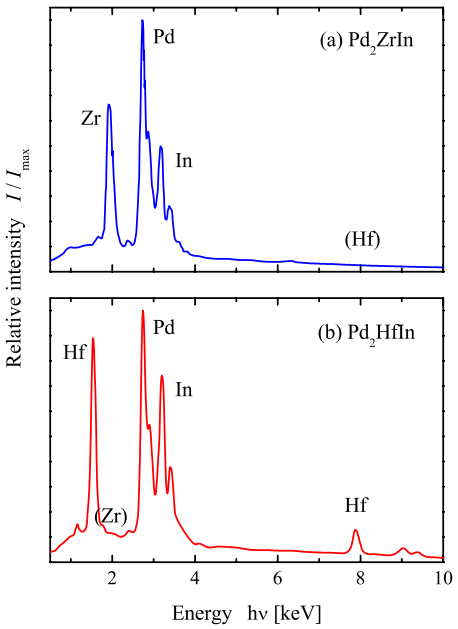

FIG. 3. (Color online) EDX spectra of (a) Pd_2ZrIn and (b) Pd_2HfIn. No cross contamination of Zr and Hf is observed.

was applied, and the sample magnetization was measured with increasing temperature. The FC magnetization was recorded subsequently in the same induction field upon cooling down to 1.8 K again. The field-dependent magnetization was recorded at a temperature of 2 K, well below the transition temperatures of all superconductors.

IV. RESULTS AND DISCUSSION

A. Pure compounds

1. Structural characterization

All compounds crystallize in the cubic $L2_1$ Heusler structure (space group $Fm\bar{3}m$), where the Wyckoff positions are $8c$ $(\frac{1}{4},\frac{1}{4},\frac{1}{4})$ for Pd atoms, $4a$ (0,0,0) for B=Zr or Hf atoms, and $4b$ $(\frac{1}{2},\frac{1}{2},\frac{1}{2})$ for C=Al or In atoms. Figure 2 shows the diffraction patterns for all pure compounds. The raw data (black) are compared to the difference between a calculated Rietveld refinement and the raw data (gray). The experimental lattice parameters as found from Rietveld refinements are given in Table I. The patterns indicate excellent phase purity for all compounds. In the case of Pd_2ZrIn, the (111) reflex is very small, and the (200) reflex is not seen at all. This is not an effect of $B2$-type disorder but is instead due to almost equal scattering factors of Pd, Zr, and In. Even in a presumably perfectly ordered $L2_1$ structure of Pd_2ZrIn, the intensity of the (200) reflex would be less than 1% of that of the (220) reflex.

Hf and Zr are very difficult to separate during purification of the elements even in high-purity materials. The used Zr is stated to contain less than 3% Hf by the manufacturer and vice versa, <3% Zr in Hf. To detect this type of cross contamination, polished disks of the materials were investigated using scanning electron microscopy with EDX. No traces of Hf were found in the Zr-containing compounds and vice versa as shown in Fig. 3. According to the methodological detection limit, the impurities of Pd_2HfIn in Pd_2ZrIn are $\leq 1\%$.

2. Calculational results

The calculated electronic structures of Pd_2ZrAl and Pd_2ZrIn are shown in Figs. 4 and 5. The electronic structure of both compounds is very similar. The hybridization gap—typical for Heusler compounds—that separates the low-lying s states from the d bands is clearly visible at around 6 eV below the Fermi energy in the energy dispersion curve as well as in the density of states of both compounds. This gap is slightly larger in Pd_2ZrIn, reflecting the larger lattice parameter as compared to Pd_2ZrAl.

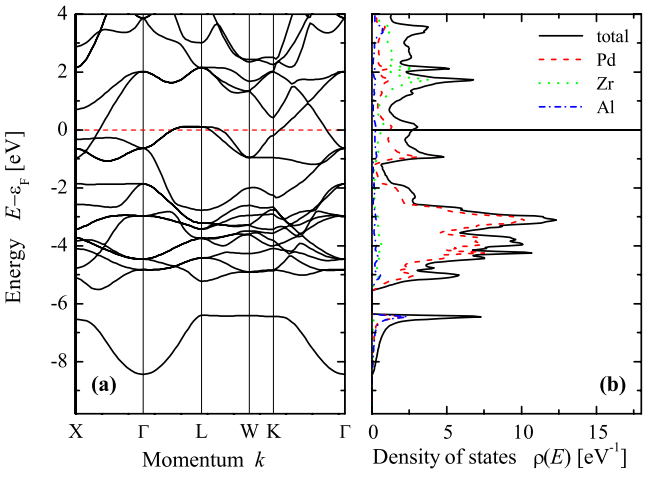

FIG. 4. (Color online) Electronic structure of Pd_2ZrAl. (a) displays the band structure and (b) the density of states. (Both were calculated using FLAPW for the optimized lattice parameter.)

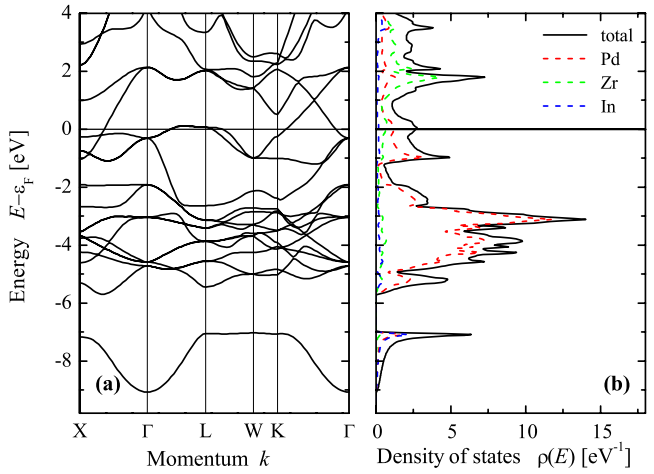

FIG. 5. (Color online) Electronic structure of Pd_2ZrIn. (a) displays the band structure and (b) the density of states. (Both were calculated using FLAPW for the optimized lattice parameter.)

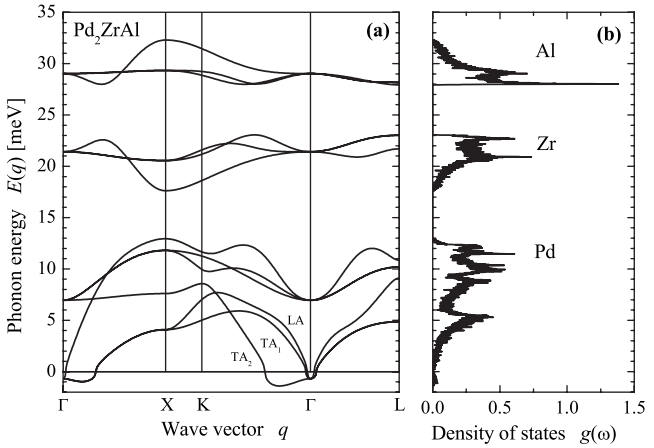

FIG. 6. Vibrational structure of Pd_2ZrAl. (a) displays the phonon dispersion and (b) the phonon density of states $g(\omega)$. Note that negative energies correspond to solutions of the wave equation with complex q values. (The calculations were performed with the optimized lattice parameter.)

Most interesting, however, is the occurrence of a van Hove singularity just above the Fermi energy at the L point. At the same time, only one rather steep, d band is crossing the Δ direction. The flat bands forming the van Hove singularity at the L point result in a maximum density of states. This maximum density emerging from the states just above ϵ_F is about 3.5 eV^{-1} in Pd_2ZrAl and thus about 0.8 eV^{-1} higher than in Pd_2ZrIn. In both compounds, the density is slightly lower directly at ϵ_F.

The energy of the states at the high-symmetry points is summarized in Table II together with the density of states $n(\epsilon_F)$ at the Fermi energy. Table II shows that the energy of the van Hove singularity at the L point is rather resistant to variation in the lattice parameter, whereas some deviations are found in the energies of the states at the Γ and X points if comparing the values calculated for the experimental and optimized lattice parameters. The density of states at the Fermi energy is slightly higher in the Zr compounds compared to the Hf compounds. Overall, no remarkable differences are noticed if comparing the compounds or the different lattice parameters used in the calculations.

Figure 6 shows the phonon dispersion and the phonon spectrum of Pd_2ZrAl. The vibronic structure exhibits four groups of vibrational states, the low-lying acoustical modes, and the high-lying optical modes. For high-symmetry directions, the set of acoustic modes (LA, TA_1, and TA_2) is nondegenerate only along Γ-K. The optical modes are threefold degenerate at Γ as is revealed in the splitting of the bands in the Σ direction. The highest optical modes originate from the Al atoms and the lowest optical modes arise from Pd [see Fig. 6(b)].

TABLE II. Energy of the van Hove singularities close to ϵ_F. The experimental lattice parameters a of the Al-containing compounds are assigned by *. All energies E are given with respect to the Fermi energy ϵ_F.

	a (Å)	$E(L)$ (meV)	$E(\Gamma)$ (meV)	$E(X)$ (meV)	$n(\epsilon_F)$ (eV^{-1})
Pd_2ZrAl	6.406*	108	−694	−317	2.6
	6.467	109	−630	−299	2.7
Pd_2ZrIn	6.623	65	−307	−270	2.7
Pd_2HfAl	6.376*	172	−643	−287	2.3
	6.436	173	−585	−272	2.4
Pd_2HfIn	6.592	136	−171	−245	2.4

The acoustical modes of Pd_2ZrAl are unstable close to the Γ point. The energies with negative values correspond to wave vectors with complex q values. This instability is most pronounced in the TA_2 mode, which is unstable over a wider range of q. Such instabilities were previously observed in Ni-based and Co-based Heusler compounds.[27,28] For the example of Ni_2TiGa, it was shown[28] that magnetic order is not a necessary condition for phonon softening to occur. Here, this fact is demonstrated for another nonmagnetic compound.

The phonon dispersion and density of Pd_2ZrIn is shown in Fig. 7, in which the density can be seen to cover a smaller range of phonon energies. Due to the higher mass of In, the splitting of the three groups of optical modes is less pronounced compared to Pd_2ZrAl. The gaps between the groups are closed or become pseudogaps.

Table III summarizes the energies of the optical phonon modes and compares the average phonon frequency $\bar{\omega} = \int \omega g(\omega) d\omega$ to the Debye temperature Θ_D. Θ_D was determined from a fit of the calculated specific heat of the phonons to a Debye model. The high-lying optical modes at about 30 meV in the Al-containing compounds do not overlap with the remainder of the phonon spectrum and appear like Einstein frequencies. In a hybrid Einstein-Debye model for Pd_2HfAl, the corresponding Einstein temperature is $\Theta_E \approx 350$ K calculated from the average phonon frequencies of that mode. The Debye temperature of Pd_2ZrAl was not clearly revealed from the fit. This is partially due to the observed phonon softening. Most probably, the clear splitting of the Zr-induced optical mode requires a hybrid model with two different Einstein temperatures to describe the specific

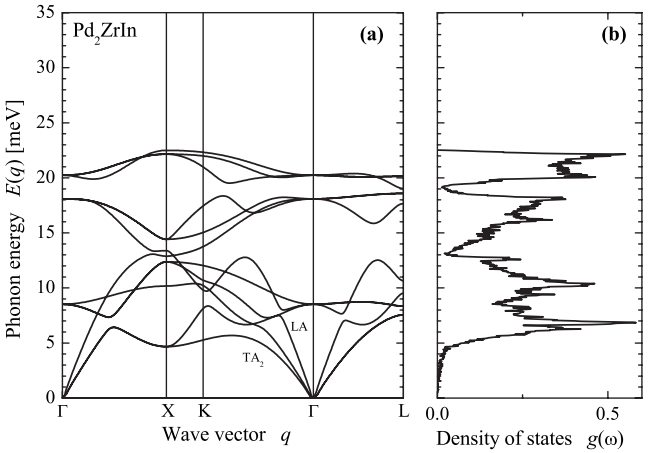

FIG. 7. Vibrational structure of Pd_2ZrIn. (a) displays the phonon dispersion and (b) the phonon density of states. (The calculations were performed with the optimized lattice parameter.)

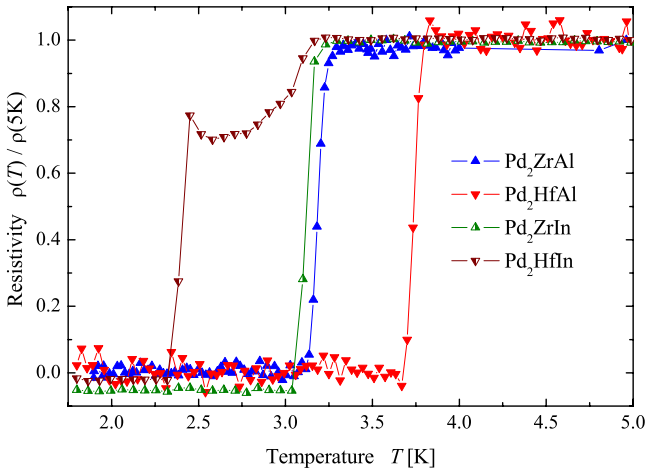

FIG. 8. (Color online) Resistive superconducting transitions of the pure compounds. Shown is the temperature-dependent resistivity in the region around T_c^{mid} for the Heusler superconductors Pd_2ZrAl, Pd_2HfAl, Pd_2ZrIn, and Pd_2HfIn.

heat correctly. The Debye temperatures of the In-containing compounds are lower compared to those with Al, as expected from the differences of the phonon spectra.

3. Resistivity

The superconducting transitions of the pure compounds were verified with temperature-dependent resistivity measurements. Figure 8 shows the resistive superconducting transitions of the pure compounds. The transition temperatures T_c^{mid} were determined by calculating the mean value of the onsets and offsets of the superconducting transitions. The values are summarized in Table IV. In the case of Pd_2HfIn, the onset of a superconducting transition can already be observed at approximately 3.1 K, but the resistivity does not drop straight to zero. This jump is then followed by the pronounced bulk superconducting transition for the Heusler compound at 2.4 K. No impurities were found in the XRD pattern of Pd_2HfIn. It is therefore concluded that this broad onset may be attributed to bulk inhomogeneities of the sample. It may be caused by an unidentified ternary or binary impurity phase below the XRD detection limit consisting of the elements Pd, Hf, and In as neither contaminations nor impurities of Zr were found in the EDX analysis.

4. Magnetic properties

The results of the temperature-dependent magnetization measurements are given in Figs. 9(a)–9(d). All compounds exhibit superconducting transitions. The onsets of these transitions are given in Table IV. Thermal irreversibilities between ZFC and FC measurements indicate that all compounds are type II superconductors. All samples show quite sharp superconducting transitions indicating low grades of impurity. However, very large differences in magnitude between ZFC and FC measurements are found in all cases indicating a reduced Meissner effect. This feature is caused by flux pinning that is attributed to bulk inhomogeneities. For all compounds, the resistive superconducting transitions appear at slightly higher temperatures as compared to the magnetization measurements. This fact is well known. The resistive transition takes place when one percolation path throughout the sample becomes superconducting. The magnetic transition requires a certain superconducting volume. The volume susceptibilities χ_V were calculated assuming a demagnetization factor of $\frac{1}{3}$ of a perfect sphere. Using this approximation for all compounds confirms bulk superconductivity. Precise statements about the superconducting vol-

TABLE III. Energetics of the optical phonon modes and average temperatures. The energy at X corresponds to the highest mode. The temperature equivalent of the mean phonon frequency $\bar{\omega}$ is given for better comparison to the Debye temperature Θ_D [note that the values with * are not accurate due to the phonon softening in Pd_2ZrAl (see Fig. 6)].

	$\hbar\omega(\Gamma)_1$ (meV)	$\hbar\omega(\Gamma)_2$ (meV)	$\hbar\omega(\Gamma)_3$ (meV)	$\hbar\omega(X)$ (meV)	$\bar{\omega}$ (K)	Θ_D (K)
Pd_2ZrAl	6.96	21.4	29.0	32.3	194*	>310*
Pd_2ZrIn	8.52	18.1	20.2	22.5	159	220
Pd_2HfAl	10.2	18.9	28.5	31.1	194	277
Pd_2HfIn	9.73	16.5	18.8	21	153	209

TABLE IV. Critical temperatures of the palladium-based Heusler superconductors. The critical temperatures T_c^{mid} of the resistivity measurements represent mean values of the superconducting onsets and offsets. The critical temperatures from the magnetization measurements T_c^{Mag} represent the onsets of the superconducting transitions.

	T_c^{Res} (K)	T_c^{Mag} (K)	H_{c1} (mT)
Pd_2ZrAl	3.2	3.1	6.0
Pd_2ZrIn	3.1	3.0	12.3
Pd_2HfAl	3.8	3.4	10.3
Pd_2HfIn	2.4	2.3	6.2

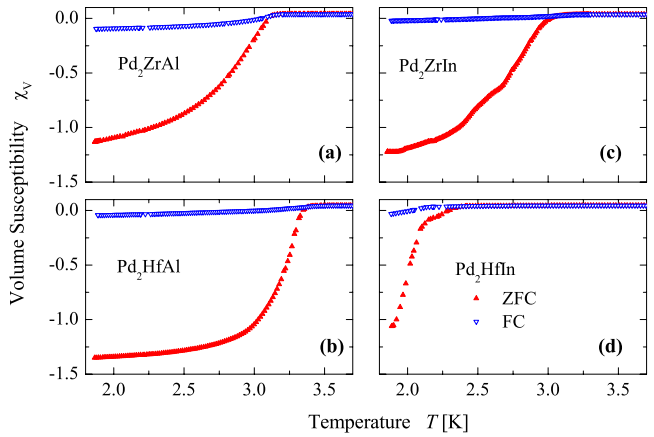

FIG. 9. (Color online) Temperature-dependent magnetization of the pure compounds. Panels (a)–(d) show the volume susceptibilities χ_V in the regions around T_c upon ZFC and FC conditions for Pd_2ZrAl, Pd_2HfAl,[12] Pd_2ZrIn, and Pd_2HfIn. The measurements were performed with magnetic induction fields $\mu_0 H$ of 2.5 mT, respectively.

umes, however, cannot be made because the measured samples do not correspond to perfect spherical or other geometrical bodies. The segregated unidentified impurity, which was found in the resistivity measurement of Pd_2HfIn, is also observed as additional structure in the corresponding temperature-dependent magnetization curve. The magnetic data of Pd_2ZrIn also exhibit small deviations. This suggests that the unidentified impurity may consist of the elements Pd and In only. Due to the higher transition temperature of Pd_2ZrIn, this effect is not visible in the corresponding resistivity measurement. The critical temperatures of both compounds may increase if formation of this impurity phase can be avoided.

Figures 10(a)–10(d) shows the field-dependent magnetizations (butterfly curves) at temperatures of 2 K in the superconducting state for all compounds. Theoretically, the

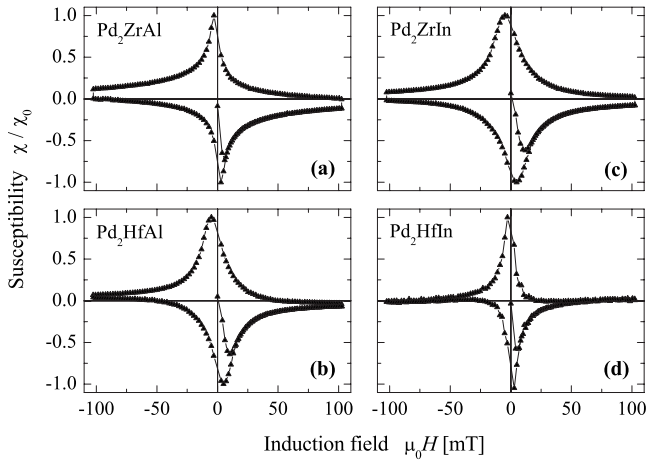

FIG. 10. Butterfly curves for Pd_2ZrAl, Pd_2HfAl,[12] Pd_2ZrIn, and Pd_2HfIn. Panels (a)–(d) show the normalized susceptibilities χ/χ_0 at temperatures of 2 K in a range from −100 to 100 mT, respectively. All curves were measured from the ZFC state.

TABLE V. Properties of the substituted palladium-based Heusler superconductors. a are the measured lattice parameters and T_c^{mid} is the critical temperatures from resistivity measurements.

	a (Å)	T_c^{mid} (K)
$Pd_2Zr_{0.9}Y_{0.1}Al$	6.432	
$Pd_2Zr_{0.9}Nb_{0.1}Al$	6.372	2.1
$Pd_2Hf_{0.75}Y_{0.25}Al$	6.393	3.2
$Pd_2Hf_{0.5}Y_{0.5}Al$	6.404	2.9

critical magnetic field H_{c1} for a certain temperature and a certain compound can be determined from the virgin curve of the field-dependent magnetization. This is not possible, however, for these intermetallic samples, because the bulk inhomogeneities lead to a more symmetric shape of the curves, which impedes accurate calculations of H_{c1}. Rough estimations provide values of H_{c1} for the compounds as presented in Table IV.

B. Substituted compounds

According to the van Hove scenario,[11] a maximum T_c should be obtained for a maximum $n(\epsilon_F)$ at ϵ_F at a given Debye frequency and Cooper-pairing interaction. For the cases of Pd_2ZrAl and Pd_2HfAl, the van Hove singularities coincide with ϵ_F when the compounds are doped with electrons. Assuming a rigid-band model and a fixed lattice parameter, the calculated electronic structure suggests that doping by about 0.1 of an electron shifts the band with the singularity at L onto ϵ_F. This may be established by substituting the group 4 element (Zr, Hf) by 10% of an element of group 5 (V, Nb) or 5% in case of group 6 elements (Cr, Mo). In a similar way, a substitution by a group 3 (Sc, Y) element will shift ϵ_F downwards to the singularity at X. To investigate the behavior of T_c upon electron doping and hole doping the solid solutions of $Pd_2B_{1-x}B'_xAl$ with B=Zr and Hf, and B'=Y, Nb, and Mo were prepared as described in Sec. III. For Pd_2ZrAl, Y and Nb could be substituted for Zr, whereas only Y could be substituted for Hf in Pd_2HfAl. Doping with Mo was not possible for either compound.

1. Structural characterization

The crystal structures of the substituted alloys were analyzed as described in Sec. III. The alloys crystallize in the cubic $L2_1$ Heusler structure (space group $Fm\bar{3}m$). With the exception of $Pd_2Hf_{0.5}Y_{0.5}Al$, none of the alloys exhibit any impurities in the XRD patterns. The experimental lattice parameters are obtained from Rietveld refinements (see Table V). The increasing and decreasing lattice parameters in the solid solutions originate from the differing atomic radii of the substituted elements. The atomic radii of Nb and Mo are smaller than those of Zr and Hf, whereas the atomic radius of

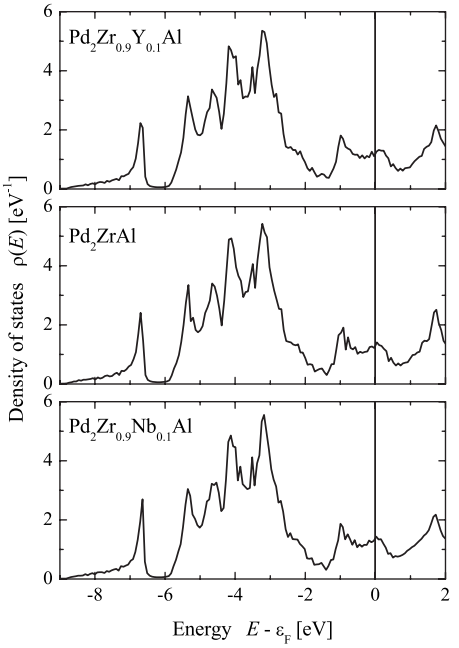

FIG. 11. Electronic structure of $Pd_2Zr_{0.9}B_{0.1}Al$, B=Y, Nb. Compared is the density of states of the pure compound to the cases of 10% substitution of Zr by Y or Nb. (Calculated by SPRKKR with the experimental lattice parameter.)

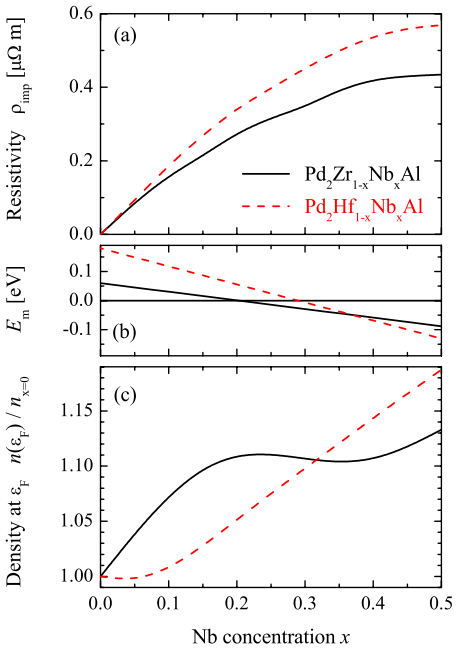

FIG. 12. (Color online) Electron doping in $Pd_2Zr_{1-x}Nb_xAl$ and $Pd_2Hf_{1-x}Nb_xAl$. (a) shows the residual resistivity due to *impurity* scattering, (b) shows the energy shift of the maximum of $n(E)$ associated with the van Hove singularity at the L point, and (c) shows the density of states at the Fermi energy relative to the density in the pure compounds with x=0. (Calculated for the *normal* conducting state by SPRKKR with the fixed lattice parameters of the pure compounds.)

Y is larger. This is reflected in the lattice parameters listed in Table V. Besides the impurities, which were found in the XRD pattern of $Pd_2Hf_{0.5}Y_{0.5}Al$, the small difference between the lattice parameters of $Pd_2Hf_{0.75}Y_{0.25}Al$ and $Pd_2Hf_{0.5}Y_{0.5}Al$ supports the conclusion that the lattice of $Pd_2Hf_{1-x}Y_xAl$ becomes saturated with Y when $0.25 \leq x \leq 0.5$. Increasing the Y concentration above this limit causes impurities to segregate. One of these impurities was identified as elemental yttrium.

2. Calculational results

Figure 11 shows a comparison between the density of states of the $Pd_2Zr_{0.9}Y_{0.1}Al$ and $Pd_2Zr_{0.9}Nb_{0.1}Al$ solid solutions and of Pd_2ZrAl in its pure form. The calculations were performed using SPRKKR and the results agree very well with the density of states from the FLAPW calculations. The solid solutions were treated in the CPA approximation. It should be noted that a band structure is no longer persistent in the random alloys due to the lack of periodicity.

Figure 11(a) shows that the maximum density of states close above ϵ_F, being indicative for the van Hove singularity at the L point, is slightly shifted to higher energies in the Y-substituted compound. This is due to underdoping of electrons. The position of the maximum is rather stable for electron doping in the Nb-containing compound [see Fig. 11(c)] in comparison to the pure Zr compound [see Fig. 11(b)]. This shows that bands do not behave completely rigid. However, a small shift of ϵ_F is evident. Adequate electron doping should thus allow the van Hove singularity to coincide with ϵ_F. In theory, the situation is rather similar for electron-doped and hole-doped Pd_2HfAl.

Figure 12 illustrates the effect of electron doping on the electronic properties for the examples of $Pd_2Zr_{1-x}Nb_xAl$ and $Pd_2Hf_{1-x}Nb_xAl$. The energy shift of the maximum of $n(E)$ associated with the van Hove singularity at the L point cannot be given more precisely due to lack of a band structure. From the fit, it is expected that the singularity coincides with ϵ_F at a Nb concentration of approximately 20 or 30% in the alloys based on Zr or Hf, respectively. The density of states $n(\epsilon_F)$ at the Fermi energy increases with increasing Nb content.

A detailed analysis of Pd_2HfAl reveals that this increase is not primary due to the shift of the maximum of the density of states arising from Pd states of the pure compound but by an increase in the density located at the Nb atoms. This reordering of the electron densities demonstrates that a rigid-band model is not directly applicable for this sort of compounds even if using a fixed lattice parameter in the calculations. Pd_2ZrAl shows an intermediate maximum of $n(\epsilon_F)$. In this case, the local density of states $n_{Pd}(\epsilon_F)$ at the Pd atoms also exhibits a maximum. Here, the Nb concentration x at the intermediate maximum of $n(x, \epsilon_F)$ corresponds to the one where the van Hove saddle point at L coincides with the Fermi energy.

In a trivial analysis, the increase in states at ϵ_F may suggest that the resistivity decreases already in the normal conducting state. This is, indeed, not the case due to the strong influence of impurity scattering in the substituted compounds. The random distribution of the Zr or Hf and Nb atoms on a common site of the lattice leads to an increase in

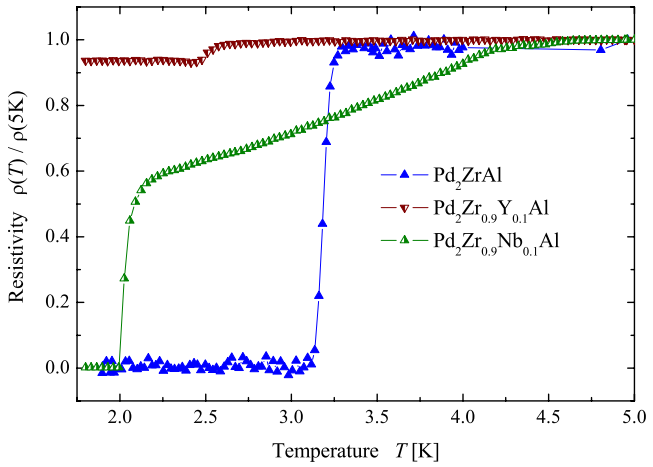

FIG. 13. (Color online) Resistive superconducting transitions for the solid solutions $Pd_2Zr_{1-x}B'_xAl$. Shown is the temperature-dependent resistivity in the region around T_c^{mid} for the pure compound Pd_2ZrAl as well as the alloys $Pd_2Zr_{0.9}Y_{0.1}Al$ and $Pd_2Zr_{0.9}Nb_{0.1}Al$.

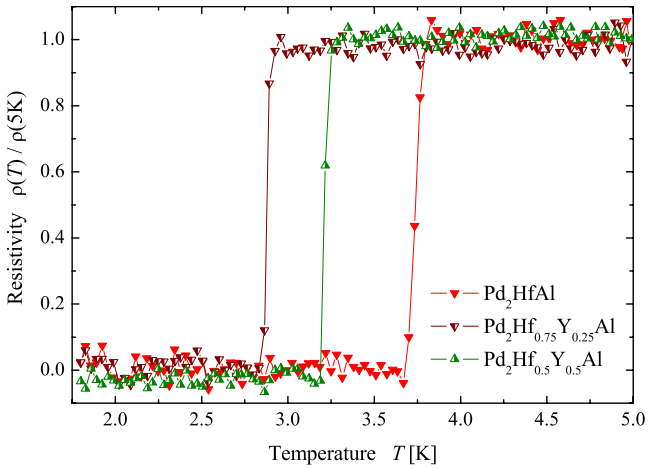

FIG. 14. (Color online) Resistive superconducting transitions for the solid solutions $Pd_2Hf_{1-x}Y_xAl$. Shown is the temperature-dependent resistivity in the region around T_c^{mid} for the pure compound Pd_2HfAl as well as the alloys $Pd_2Hf_{0.75}Y_{0.25}Al$ and $Pd_2Hf_{0.5}Y_{0.5}Al$.

the resistivity as is also observed for simple binary alloys such as $Pd_{1-x}Ag_x$.[29,30] It is conceivable that reordering of charges and/or impurity scattering prevent an increase in the superconducting transition temperature.

3. Resistivity

All solid solutions were investigated with respect to superconductivity in temperature-dependent resistivity measurements as described in Sec. III. The corresponding critical temperatures T_c^{mid} are given in Table V. Figure 13 shows the resistivity measurement of Pd_2ZrAl in comparison to the alloys $Pd_2Zr_{0.9}Y_{0.1}Al$ and $Pd_2Zr_{0.9}Nb_{0.1}Al$. A superconducting transition was only found in $Pd_2Zr_{0.9}Nb_{0.1}Al$ (T_c^{mid}=2.1 K). In this alloy, resistivity already begins to decrease at approximately 4.1 K. This may be attributed to a superconducting impurity phase below the detection limit of XRD. This phase may be a disordered cubic *A*15 material.[31] Some of these are known to exhibit superconducting transitions around 4 to 5 K. $Pd_2Zr_{0.9}Y_{0.1}Al$ does not show a superconducting transition. A small drop in resistivity occurs at approximately 2.6 K, but this does not correspond to a bulk superconducting transition. Most probably, this drop is caused by small superconducting paths in regions with lower yttrium contents throughout the inhomogeneous bulk sample. Figure 14 shows the temperature-dependent resistivity of Pd_2HfAl in comparison to the alloys $Pd_2Hf_{0.75}Y_{0.25}Al$ and $Pd_2Hf_{0.5}Y_{0.5}Al$. Superconducting transitions are observed in both alloys but the transition temperature decreases with increasing yttrium concentration.

Maximum transition temperatures were expected for electron-doped Pd_2ZrAl and Pd_2HfAl according to the van Hove scenario. For Pd_2HfAl, no conclusion can be drawn about the possibility of electron doping and increasing T_c because only Y was incorporated successfully into the unit cell of Pd_2HfAl. This hole doping led to a decrease in T_c with increasing Y content as expected from the electronic structure. For Pd_2ZrAl, hole doping with 10% of Y led to destruction of superconductivity, and the superconducting transition is lowered in the alloy $Pd_2Zr_{0.9}Nb_{0.1}Al$ as compared to Pd_2ZrAl. The expected behavior was thus not found. Nonmagnetic scattering should not suppress superconductivity by itself according to Anderson's theorem.[32] It was, however, shown that enhanced disorder leads to spatial fluctuations of the superconducting gap Δ and eventually to suppression of the superconducting state.[33] Thus, a Nb concentration of 10% manifestly provokes a degree of disorder, which is sufficient to reduce T_c considerably. Electron-doping experiments with the cubic *A*15 superconductors led to similar results, where T_c is very often lowered upon electron doping or hole doping via element substitution.[34]

V. SUMMARY AND CONCLUSIONS

Using *ab-initio* calculations as a basis, the Heusler compounds Pd_2ZrAl, Pd_2HfAl, Pd_2ZrIn, and Pd_2HfIn have been identified as prospects for superconductivity according to the van Hove scenario. Resistivity and magnetization measurements provided evidence that all compounds are type II bulk superconductors with transition temperatures in the range of 2.4–3.8 K. Following the van Hove scenario, solid solutions of $Pd_2B_{1-x}B'_xAl$ with B=Zr and Hf, and B'=Y, Nb, and Mo were synthesized to investigate the dependence of superconducting properties on the valence electron concentration and thus the density of states at the Fermi energy. Although the incorporation of some elements was possible for both compounds Pd_2ZrAl and Pd_2HfAl, superconductivity was suppressed in all solid solutions as compared to the pure compounds. The rather sizable amounts of the substituents used here provoked a degree of disorder beyond the validity of the Anderson theorem. Instead of shifting the van Hove singularities to ϵ_F they caused suppressions of the superconducting state.

ACKNOWLEDGMENTS

This work has been funded by the DFG (German Research Foundation) through the "*Condensed Matter Systems with Variable Many-Body Interactions*" Collaborative Research Center (Transregio Grant No. SFB/TRR 49). The authors thank Changhai Wang and Andrei Gloskovskii for the EDX analysis and Gerhard Jakob for suggestions and fruitful discussions. The authors are also very grateful to P. Blaha (Vienna, Austria), H. Ebert (Munich), and their groups for development and providing the computer codes.

[1] F. Heusler, Verhandl. DPG **5**, 219 (1903).
[2] C. Felser, G. H. Fecher, and B. Balke, Angew. Chem. Int. Ed. **46**, 668 (2007).
[3] H. C. Kandpal, G. H. Fecher, and C. Felser, J. Phys. D **40**, 1507 (2007).
[4] T. Marukame, T. Ishikawa, S. Hakamata, K. Matsuda, T. Uemura, and M. Yamamoto, Appl. Phys. Lett. **90**, 012508 (2007).
[5] N. Tezuka, N. Ikeda, S. Sugimoto, and K. Inomata, Appl. Phys. Lett. **89**, 252508 (2006).
[6] M. Ishikawa, J. L. Jorda, and A. Junod, in *Superconductivity in d- and f-Band Metals*, edited by W. Buckel and W. Weber (Kernforschungszentrum, Karlsruhe, Germany, 1982).
[7] J. H. Wernick, G. W. Hull, J. E. Bernardini, and J. V. Waszczak, Mater. Lett. **2**, 90 (1983).
[8] H. A. Kierstead, B. D. Dunlap, S. K. Malik, A. M. Umarji, and G. K. Shenoy, Phys. Rev. B **32**, 135 (1985).
[9] R. N. Shelton, L. S. Hausermann-Berg, M. J. Johnson, P. Klavins, and H. D. Yang, Phys. Rev. B **34**, 199 (1986).
[10] L. van Hove, Phys. Rev. **89**, 1189 (1953).
[11] C. Felser, J. Solid State Chem. **160**, 93 (2001).
[12] J. Winterlik, G. H. Fecher, and C. Felser, Solid State Commun. **145**, 475 (2008).
[13] J. Winterlik, G. H. Fecher, C. Felser, M. Jourdan, K. Grube, F. Hardy, H. von Löhneysen, K. L. Holman, and R. J. Cava, Phys. Rev. B **78**, 184506 (2008).
[14] G. Gladstone, M. A. Jensen, and J. R. Schrieffer, in *Superconductivity*, edited by R. D. Parks, (Dekker, New York, 1969), Vol. 2.
[15] P. Blaha, K. Schwarz, P. Sorantin, and S. Tricky, Comput. Phys. Commun. **59**, 399 (1990).
[16] P. Blaha, K. Schwarz, G. K. H. Madsen, D. Kvasnicka, and J. Luitz, *WIEN2k, An Augmented Plane Wave+Local Orbitals Program for Calculating Crystal Properties* (Technische Universitaet Wien, Wien, Austria, 2001).
[17] K. Parlinski, Software PHONON, 2006.
[18] H. Ebert, in *Lecture Notes in Physics*, edited by H. Dreysse (Springer, New York, 1999), Vol. 535, pp. 191–246.
[19] H. Ebert, The Munich SPR-KKR package, Version 3.6, 2005 (http://olymp.cup.uni-muenchen.de/ak/ebert/SPRKKR).
[20] J. P. Perdew, K. Burke, and M. Ernzerhof, Phys. Rev. Lett. **77**, 3865 (1996).
[21] S. H. Vosko and L. Wilk, Phys. Rev. B **22**, 3812 (1980).
[22] S. H. Vosko, L. Wilk, and M. Nusair, Can. J. Phys. **58**, 1200 (1980).
[23] D. M. Teter, G. V. Gibbs, M. B. Boisen, D. C. Allan, and M. P. Teter, Phys. Rev. B **52**, 8064 (1995).
[24] P. Mohn, P. Blaha, and K. Schwarz, J. Magn. Magn. Mater. **140-144**, 183 (1995).
[25] S. C. Lee, T. D. Lee, P. Blaha, and K. Schwarz, J. Appl. Phys. **97**, 10C307 (2005).
[26] J. P. Perdew, A. Ruzsinszky, G. I. Csonka, O. A. Vydrov, G. E. Scuseria, L. A. Constantin, X. Zhou, and K. Burke, Phys. Rev. Lett. **100**, 136406 (2008).
[27] C. Bungaro, K. M. Rabe, and A. Dal Corso, Phys. Rev. B **68**, 134104 (2003).
[28] A. T. Zayak, P. Entel, K. M. Rabe, W. A. Adeagbo, and M. Acet, Phys. Rev. B **72**, 054113 (2005).
[29] W. H. Butler and G. M. Stocks, Phys. Rev. B **29**, 4217 (1984).
[30] P. Weinberger, *Electron Scattering Theory for Ordered and Disordered Matter* (Clarendon, Oxford, 1990).
[31] H. Gutfreund, M. Weger, and O. Entin-Wohlman, Phys. Rev. B **31**, 606 (1985).
[32] P. W. Anderson, J. Phys. Chem. Solids **11**, 26 (1959).
[33] M. Ma and P. A. Lee, Phys. Rev. B **32**, 5658 (1985).
[34] S. V. Vonsovsky, Y. A. Izyumov, and E. Z. Kurmaev, *Superconductivity of Transition Metals* (Springer-Verlag, Berlin, Germany, 1982).